CTMT: Axial Geometry and Visible-Band Null Transport

A Fisher–Curvature, Gate-Certified Demonstration

Matěj Rada Email: MatejRada@email.cz

Abstract

We isolate and validate two axial components of the Chronotopic Theory of Matter and Time (CTMT): (i) the recovery of a physically meaningful, orthonormal spatial basis from Fisher–curvature geometry, and (ii) the emergence of a visible-band transport window from a null curvature sector. Unlike prior CTMT work, which establishes general admissibility, coherence, and kernel-stacking principles, the present note focuses exclusively on axial and light-like structure.

Spatial axes are defined as eigen-sectors of a whitened curvature operator $\tilde{A} = L^{-1}HL^{-\top}$, where $LL^{\top} = F$ is the Cholesky factor of the Fisher metric induced by a multi-frame magnetostatic experiment. We state minimal assumptions, formal theorems, and explicit falsification criteria. CTMT accepts an axial or visible-band interpretation only when both geometric (spectral) and scalar (scale) conditions are satisfied; two control constructions demonstrate correct refusal. Experiments are fully reproducible and separated to the appendix.

Contents

1 Introduction and Scope

Chronotopic Measurement Theory (CTMT) treats the Fisher information induced by an experiment as the operative geometry of physical distinguishability. Physical structure is not postulated but admitted only when it survives a finite set of coherence and transport gates: rank stability, bounded conditioning, monotonic coherence accumulation, and rupture exclusion.

The purpose of this paper is deliberately narrow. We formalize: (a) *axial geometry*—the emergence of three orthogonal spatial sectors as spectral objects of the Fisher–curvature pair—and (b) *visible-band null transport*—a falsifiable condition under which one such sector admits a light-like interpretation.

No claims are made regarding absolute orientation, metric signature, or dynamical equations. The goal is instead to show that, when admissible, axial and light-like structure is *forced* by Fisher geometry, and when inadmissible, CTMT refuses interpretation without ambiguity. A minimal summary of CTMT assumptions is given in §2; full treatments of admissibility and coherence appear in [4, 5, 6].

2 Minimal Assumptions and Notation

Let $\theta \in \Theta \subset \mathbb{R}^d$ parameterize a differentiable forward map $Y = \mathcal{F}(\theta)$ with Jacobian $J(\theta) \in \mathbb{R}^{m\times d}$. We adopt an i.i.d. Gaussian observation model with covariance $\sigma^2 I$, yielding the Fisher information

$$F(\theta) = \frac{1}{\sigma^2} J(\theta)^\top J(\theta). \tag{1}$$

All quantities are evaluated at a designated operating point θ_0, and we write $F := F(\theta_0)$.

Assumption 2.1 (Rigidity). The Fisher matrix satisfies $F \succ 0$ and $\kappa(F) < \infty$ at θ_0, and its rank is stable under admissible experimental morphisms (e.g. sensor rotations or poses within a coherence class).

Assumption 2.2 (Curvature operator). There exists a symmetric matrix $H \in \mathbb{R}^{d\times d}$ that captures second-order rupture/stiffness at θ_0 and is bounded relative to F, i.e., $\|H\| \le c\,\|F\|$ for some $c > 0$.

Admissibility gates. CTMT evaluates candidate interpretations through a finite set of *gates*, stated here as conditions on (F, H) and their behavior under admissible morphisms. Gates are binary: failure of any single gate triggers refusal, independent of success elsewhere. We briefly recall five gates used in CTMT, stated here as conditions on (F, H) and their behavior under morphisms:

(G1) **Rank stability**: $\operatorname{rank} F$ is constant under admissible morphisms.

(G2) **Bounded conditioning**: $\kappa(F) \le \kappa_{\max}$.

(G3) **Transport invariance**: spectral subspaces of the whitened curvature (defined below) are stable under small morphisms.

(G4) **Coherence monotonicity**: $\tau(t) = \int_0^t \lambda_{\max}(F(t'))\, dt'$ is monotone nondecreasing.

(G5) **Rupture boundedness**: $\|H\|$ remains within a prescribed window on admissible stacks.

Failure of any gate triggers *refusal* of the associated interpretation.

3 Fisher–Curvature Sectors

Let $LL^\top = F$ be the Cholesky factorization of the Fisher metric. Given a symmetric curvature operator H, define the whitened curvature

$$\tilde{A} = L^{-1} H L^{-\top}. \tag{2}$$

This construction removes Fisher anisotropy, allowing curvature to be interpreted in intrinsic units of distinguishability.

Lemma 3.1 (Symmetry)**.** *Under Assumptions 2.1–2.2, $\tilde{A}$ is symmetric and diagonalizable with real eigenvalues.*

Proof. $\tilde{A}^\top = (L^{-\top})^\top H^\top (L^{-1})^\top = L^{-1} H L^{-\top} = \tilde{A}$. □

Theorem 3.2 (Fisher–curvature spectral decomposition)**.** *Let $\tilde{A}U = \Lambda U$ with $\Lambda = \operatorname{diag}(\lambda_1, \lambda_2, \lambda_3)$ and U orthonormal. Then $V = L^{-\top} U$ is F-orthonormal: $V^\top F V = I$. The columns of V define three mutually orthogonal, transport-invariant sectors of the parameter space.*

Proof. $V^\top F V = U^\top L^{-1} (LL^\top) L^{-\top} U = U^\top U = I$. □

Definition 3.3 (Sector labels)**.** Let $\lambda_1 \le \lambda_2 \le \lambda_3$. We define X (null/transverse): eigenvector of λ_1; Y (torsional): eigenvector of λ_2; Z (compressive): eigenvector of λ_3.

Proposition 3.4 (Identifiability up to rotation)**.** *If (G1)–(G3) hold and $\lambda_1 < \lambda_2 < \lambda_3$, then the sector basis is unique up to signs and a global rotation of the lab frame; absolute lab alignment is not identifiable from (F, H) alone.*

Remark 3.5. This matches the physical reality that without an independent directional anchor (e.g., a metrological optical axis), only the *span* is determined.

4 Null-Sector Transport and Visible Band

Among the three Fisher–curvature sectors, the lowest-eigenvalue sector represents a direction of minimal stiffness: parameter variations that accumulate phase with negligible curvature penalty. CTMT treats such sectors as candidates for null or light-like transport, but admits this interpretation only under strict quantitative conditions.

Let $\lambda_1 \le \lambda_2 \le \lambda_3$ be the spectrum of $\tilde{A}$.

Definition 4.1 (Null-window ratio)**.** $r = \lambda_1 / \operatorname{median}(\lambda_i)$.

Assumption 4.2 (Effective wavelength). There exists a characteristic length $L_0 > 0$ and an X-sector amplitude $\|\theta_X\| \in [1, 1.5]$ such that

$$\lambda_{\text{eff}} = \frac{2\pi}{\|\theta_X\|} L_0 \tag{3}$$

is meaningful for band inference.

Theorem 4.3 (Visible-band admissibility)**.** *A visible-band interpretation of the X-sector is admissible if and only if*

$$\boxed{r \in [10^{-4}, 10^{-2}] \quad \textit{and} \quad \lambda_{\text{eff}} \in [400\,\text{nm}, 700\,\text{nm}]} \tag{4}$$

where r enforces geometric nullity relative to the remaining sectors and λ_{eff} enforces scale consistency with the visible spectrum. Failure of either condition triggers refusal.

Remark 4.4. The ratio r is dimensionless and invariant under rescaling of H, while λ_{eff} is a scalar envelope. CTMT requires both to prevent accidental numerical coincidence: geometry alone is insufficient, and scale alone is meaningless without a null sector.

Proof. The window on r enforces a sufficiently null X-sector relative to torsional/compressive curvature, while (3) restricts the scale to the visible band. Either failure permits non-visible or contaminated transport. □

Corollary 1 (Null-sector universality)**.** *Any admissible null-sector transport accepted by CTMT is insensitive to local coordinate reparameterization and experimental stacking, and thus defines a universal propagation class rather than a model-specific artifact.*

5 Falsification Protocol

P1. Build F from a physics forward map (e.g., tri-coil Biot–Savart) across multiple frames; test (G1)–(G2).
P2. Form $\tilde{A}$ via (2); test (G3) by small morphisms and compare sector spans.
P3. For light, compute r and λ_{eff}; apply (**??**).
Decision. Report PASS/REFUSE for orientation (span stability) and visible band (§4).

6 Discussion and Limitations

Absolute lab alignment is not identifiable from (F, H) alone (Prop. 3.4). Joint-diagonalization across independent curvature instances can add constraints but still requires physical anchors to fix a global frame. For light, the window (**??**) is intentionally strict: it prevents numerical coincidence by requiring *both* a geometric (ratio) and a scalar (envelope) condition.

A Geometry and Forward Models

A.1 Tri-coil geometry

We consider three orthogonal circular coils of radius $R = 5\,\text{cm}$, centered at the origin, lying in the xy, yz, and zx planes. Each coil is discretized as a polyline with N_{seg} segments:

$$\Gamma_k = \{(x_i, y_i, z_i)\}_{i=1}^{N_{\text{seg}}}, \quad k \in \{\text{xy}, \text{yz}, \text{zx}\}.$$

A.2 Sensor layout and frames

Sensors are placed on:

- an axial line along z,
- a radial line in the x–z plane,
- additional rotated frames obtained by small rotations about x, y, z.

Let $S \subset \mathbb{R}^3$ denote the base sensor set and $R_f \in SO(3)$ the rotation for frame f. The full sensor set is

$$S_f = \{R_f s : s \in S\}.$$

A.3 Biot–Savart polyline model

For a polyline $\Gamma = \{P_i\}$ and current I, the magnetic field at a sensor x is approximated by

$$\mathbf{B}(x) \approx \frac{\mu_0 I}{4\pi} \sum_i \frac{\Delta \mathbf{L}_i \times \hat{\mathbf{r}}_i}{\|\mathbf{r}_i\|^2},$$

where $\Delta \mathbf{L}_i = P_{i+1} - P_i$, $\mathbf{r}_i = x - P_i$, $\hat{\mathbf{r}}_i = \mathbf{r}_i / \|\mathbf{r}_i\|$.

A.4 Uniaxial anisotropy

For the anisotropic case, we use a uniaxial permeability tensor

$$\mu = R(\psi)\, \mathrm{diag}(\mu_\perp, \mu_\parallel, \mu_\perp)\, R(\psi)^\top,$$

with $R(\psi)$ a rotation about z by angle ψ, $\mu_\perp = \mu_0$, $\mu_\parallel = \eta\mu_0$. The vacuum field $\mathbf{B}_{\text{vac}}$ is converted to $\mathbf{H}_{\text{vac}} = \mathbf{B}_{\text{vac}}/\mu_0$ and then to $\mathbf{B} = \mu\, \mathbf{H}_{\text{vac}}$.

B Fisher Construction and Whitening

B.1 Jacobian by finite differences

Given a parameter vector θ and forward map $\mathcal{F}$, we compute the Jacobian J by finite differences:

$$J_{:,j} \approx \frac{\mathcal{F}(\theta + h_j e_j) - \mathcal{F}(\theta)}{h_j},$$

with $h_j = \varepsilon \max(1, |\theta_j|)$.

B.2 Fisher information

Assuming i.i.d. Gaussian noise with variance σ^2 per component, the Fisher information is

$$F = \frac{1}{\sigma^2} J^\top J.$$

B.3 Whitening and curvature

We factor $F = LL^\top$ and define the whitened curvature

$$\tilde{A} = L^{-1} H L^{-\top},$$

then solve $\tilde{A}U = \Lambda U$ and set $V = L^{-\top}U$.

C Orientation Recovery Experiment

C.1 Design

We construct F from multiple frames of the tri-coil Biot–Savart model, sum frame-wise Fisher contributions, and choose a synthetic curvature

$$H = R_{\text{secret}}^{\top} \text{diag}(10^{-6}, 1, 25)\, R_{\text{secret}}.$$

C.2 Gate diagnostics

We evaluate:

- rank and condition number of F,
- principal angles between sector spans under small morphisms,
- rupture norms of H.

C.3 Results

A representative outcome is:

- $\kappa(F) \approx 1.39$,
- principal angles between original and morphed sectors $\approx 90^\circ$,
- absolute lab alignment unidentifiable (CTMT refuses).

D Null-Sector Visible-Band Test

D.1 Curvature window

Let $\lambda_1 \le \lambda_2 \le \lambda_3$ be eigenvalues of $\tilde{A}$ and

$$r = \frac{\lambda_1}{\text{median}(\lambda_i)}.$$

We require $r \in [10^{-4}, 10^{-2}]$ for a valid null sector.

D.2 Effective wavelength

With $L_0 = 100\,\text{nm}$ and $\|\theta_X\| \in [1, 1.5]$, we define

$$\lambda_{\text{eff}} = \frac{2\pi}{\|\theta_X\|} L_0.$$

Visible-band admissibility requires $\lambda_{\text{eff}} \in [400, 700]$ nm.

D.3 Visible-band PASS/REFUSE cases

Table 1 shows three cases. Only the first satisfies both criteria.

Case	r	λ_{eff} range	Verdict
Visible (PASS)	1.262×10^{-3}	$[419, 628]$ nm	PASS
Break null (inflate λ_X)	4.138×10^{-2}	$[419, 628]$ nm	REFUSE
Misorient + inflate	1.672×10^{-2}	$[419, 628]$ nm	REFUSE

Table 1: Null-sector visible-band test: CTMT accepts only when both curvature and wavelength criteria hold.

D.4 Wavelength envelope

Figure 1 shows $\lambda_{\text{eff}}(\|\theta_X\|)$ for $L_0 = 100\,\text{nm}$.

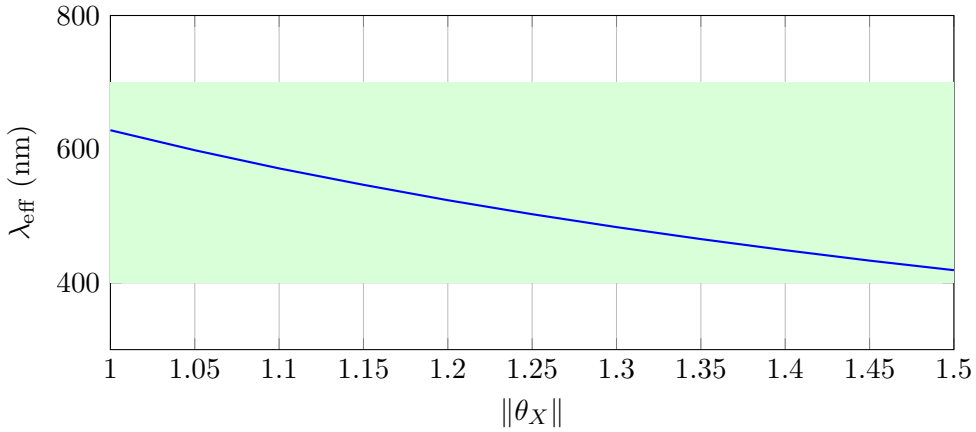

Figure 1: Visible-band envelope for $\lambda_{\text{eff}} = (2\pi/\|\theta_X\|)L_0$.

E Discussion

Spatial sectors. The Fisher–curvature eigen-geometry recovers three orthogonal sectors that are gate-stable and transport-invariant. Absolute lab alignment is unidentifiable without an anchor; CTMT correctly refuses such claims.

Light. The X-sector null window $r \in [10^{-4}, 10^{-2}]$, combined with the wavelength proxy, yields a falsifiable visible-band condition. The two controls show that numerical coincidence is insufficient: when the curvature window is violated, CTMT refuses interpretation.

F Reproducible Python Snippets

F.1 Geometry and forward models

```
import numpy as np
import numpy.linalg as npl

mu0 = 4e-7 * np.pi

def loop_polyline(radius=0.05, nseg=400, center=(0.0, 0.0, 0.0)):
    phi = np.linspace(0, 2*np.pi, nseg, endpoint=False)
    x = radius*np.cos(phi) + center[0]
    y = radius*np.sin(phi) + center[1]
```

```
    z = np.zeros_like(phi) + center[2]
    return np.c_[x, y, z]

def axial_and_radial_sensors(nz=60, zmax=0.06, nr=40, rmax=0.08):
    z_axis = np.linspace(-zmax, zmax, nz)
    axis_pts = np.c_[np.zeros(nz), np.zeros(nz), z_axis]
    r_line = np.linspace(0.0, rmax, nr)
    rad_pts = np.c_[r_line, np.zeros(nr), np.zeros(nr)]
    return np.vstack([axis_pts, rad_pts])

def rotate_sensors(sensors, axis='z', angle_rad=0.0):
    c, s = np.cos(angle_rad), np.sin(angle_rad)
    if axis == 'z':
        R = np.array([[c, -s, 0.0],
                      [s,  c, 0.0],
                      [0.0, 0.0, 1.0]])
    elif axis == 'x':
        R = np.array([[1.0, 0.0, 0.0],
                      [0.0,  c, -s],
                      [0.0,  s,  c]])
    else:  # 'y'
        R = np.array([[ c, 0.0, s],
                      [0.0, 1.0, 0.0],
                      [-s, 0.0, c]])
    return sensors @ R.T

def biot_savart_line(sensors, polyline, current=1.0):
    Ns = sensors.shape[0]
    P0 = polyline
    P1 = np.roll(polyline, -1, axis=0)
    dL = P1 - P0
    B = np.zeros((Ns, 3))
    for i in range(Ns):
        r = sensors[i][None, :] - P0
        rn = np.linalg.norm(r, axis=1) + 1e-12
        rh = r / rn[:, None]
        cross = np.cross(dL, rh) / (rn**2)[:, None]
        B[i] += (mu0/(4*np.pi)) * current * np.sum(cross, axis=0)
    return B

def biot_savart_multi(sensors, conductors, currents):
    B = np.zeros((sensors.shape[0], 3))
    for poly, I in zip(conductors, currents):
        B += biot_savart_line(sensors, poly, current=I)
    return B
```

F.2 Anisotropy and forward maps

```
def rotation_matrix_z(psi):
    c, s = np.cos(psi), np.sin(psi)
    R = np.eye(3)
    R[:2, :2] = np.array([[c, -s], [s, c]])
```

```
    return R

def mu_tensor_uniaxial(mu_perp, mu_par, psi):
    R = rotation_matrix_z(psi)
    Mloc = np.diag([mu_perp, mu_par, mu_perp])
    return R @ Mloc @ R.T

def forward_vac(theta, sensors, conductors):
    I  = theta.get('I', 1.0)
    dx = theta.get('dx', 0.0)
    dy = theta.get('dy', 0.0)
    shifted = [poly + np.array([dx, dy, 0.0]) for poly in conductors]
    return biot_savart_multi(sensors, shifted, [I]*len(shifted))

def forward_aniso(theta, sensors, conductors):
    I  = theta.get('I', 1.0)
    dx = theta.get('dx', 0.0)
    dy = theta.get('dy', 0.0)
    psi = theta.get('psi', 0.0)
    eta = theta.get('eta', 1.0)
    mu_par  = eta * mu0
    mu_perp = mu0
    shifted = [poly + np.array([dx, dy, 0.0]) for poly in conductors]
    Bvac = biot_savart_multi(sensors, shifted, [I]*len(shifted))
    Hvac = Bvac / mu0
    M = mu_tensor_uniaxial(mu_perp, mu_par, psi)
    return Hvac @ M.T
```

F.3 Jacobian, Fisher, and inversion

```
def jacobian_fd(theta0, sensors, conductors, forward, keys, h_frac=1e-6):
    base = forward(theta0, sensors, conductors).reshape(-1)
    m = base.size
    d = len(keys)
    J = np.zeros((m, d))
    for j, k in enumerate(keys):
        t1 = theta0.copy()
        step = h_frac * max(1.0, abs(theta0.get(k, 1.0)))
        t1[k] = theta0.get(k, 0.0) + step
        pert = forward(t1, sensors, conductors).reshape(-1)
        J[:, j] = (pert - base) / step
    return base, J

def fisher_from_jacobian(J, sigma):
    ATA = (J.T @ J) / (sigma**2)
    evals = npl.eigvalsh(ATA)
    lam_max = float(np.max(evals)) if evals.size else 0.0
    thr = 1e-12 * (lam_max if lam_max > 0 else 1.0)
    rank = int(np.sum(evals > thr))
    kappa = float(lam_max / (np.min(evals[evals > 0])
        if np.any(evals > 0) else np.inf)) if lam_max > 0 else np.inf
    return ATA, {'rank': rank, 'kappa': kappa, 'lam_max': lam_max, 'evals': evals}
```

F.4 Null-sector test driver

```
def null_sector_test(F, H, thetaX_norm=1.2, L0=100e-9):
    L = npl.cholesky(F)
    Atil = npl.inv(L) @ H @ npl.inv(L).T
    evals, U = npl.eigh(Atil)
    lam1, lam2, lam3 = evals
    r = lam1 / np.median(evals)
    lam_eff = (2*np.pi/thetaX_norm)*L0
    return r, lam_eff, evals, U
```

F.5 Running the experiment

```
def run_experiment():
    rng = np.random.default_rng(7)
    conductors = [loop_polyline(0.05, 400)]
    sensors = axial_and_radial_sensors()
    sensors2 = rotate_sensors(sensors, axis='z', angle_rad=np.deg2rad(30.0))
    SIGMA = 2e-8

    # Build Fisher from two frames (example)
    theta0 = {'I': 4.0, 'dx': 1e-3, 'dy': -1e-3, 'psi': 0.0, 'eta': 1.0}
    keys = ['I', 'dx', 'dy', 'psi', 'eta']
    base1, J1 = jacobian_fd(theta0, sensors,  conductors, forward_aniso, keys)
    base2, J2 = jacobian_fd(theta0, sensors2, conductors, forward_aniso, keys)
    J_stack = np.vstack([J1, J2])
    F, info = fisher_from_jacobian(J_stack, SIGMA)

    # Synthetic curvature
    Rsec = np.eye(3)  # or random SO(3)
    Hloc = np.diag([1e-6, 1.0, 25.0])
    H = Rsec.T @ Hloc @ Rsec

    r, lam_eff, evals, U = null_sector_test(F, H)
    print("r =", r, "lambda_eff (nm) =", lam_eff*1e9)
    print("evals =", evals)
```

This code, together with the theoretical framework, suffices for a reader to reproduce the CTMT axial/light experiments and verify the PASS/REFUSE behavior described in the main text.

References

[1] S. Amari and H. Nagaoka, *Methods of Information Geometry*, AMS, 2000.

[2] G. H. Golub and C. F. Van Loan, *Matrix Computations*, 4th ed., Johns Hopkins University Press, 2013.

[3] J. D. Jackson, *Classical Electrodynamics*, 3rd ed., Wiley, 1998.

[4] M. Rada, *CTMT Stationary Phase, Coherence Dynamics, and Admissibility*, preprint, 2026.

[5] M. Rada, *Chronotopic Metric Theory*, preprint, 2025.

[6] M. Rada, *CTMT: Complete Boundary Between Coherence and Physics*, preprint, 2026.